



Article

Anisotropy of the In-Plane and Out-of-Plane Resistivity and the Hall Effect in the Normal State of Vicinal-Grown $\text{YBa}_2\text{Cu}_3\text{O}_{7-\delta}$ Thin Films

Gernot Heine¹, Wolfgang Lang^{1,*} , Roman Rössler² and Johannes D. Pedarnig² ¹ Faculty of Physics, University of Vienna, Boltzmanngasse 5, A-1090 Wien, Austria; Gernot.Heine@bev.gv.at² Institute of Applied Physics, Johannes-Kepler-University Linz, Altenbergerstrasse 69, A-4040 Linz, Austria; Roman.Roessler@voestalpine.com (R.R.); Johannes.Pedarnig@jku.at (J.D.P.)

* Correspondence: wolfgang.lang@univie.ac.at

Abstract: The resistivity and the Hall effect in the copper-oxide high-temperature superconductor $\text{YBa}_2\text{Cu}_3\text{O}_{7-\delta}$ (YBCO) are remarkably anisotropic. Using a thin film of YBCO grown on an off-axis cut SrTiO_3 substrate allows one to investigate these anisotropic transport properties in a planar and well-defined sample geometry employing a homogeneous current density. In the normal state, the Hall voltage probed parallel to the copper-oxide layers is positive and strongly temperature dependent, whereas the out-of-plane Hall voltage is negative and almost temperature independent. The results confirm previous measurements on single crystals by an entirely different measurement method and demonstrate that vicinal thin films might be also useful for investigations of other layered nanomaterials.

Keywords: vicinal films; copper-oxide superconductors; Hall effect; resistivity; anisotropy



Citation: Heine, G.; Lang, W.; Rössler, R.; Pedarnig, J.D. Anisotropy of the In-Plane and Out-of-Plane Resistivity and the Hall Effect in the Normal State of Vicinal-Grown $\text{YBa}_2\text{Cu}_3\text{O}_{7-\delta}$ Thin Films. *Nanomaterials* **2021**, *11*, 675. <https://doi.org/10.3390/nano11030675>

Academic Editor: Andrey B. Evlyukhin

Received: 3 February 2021

Accepted: 5 March 2021

Published: 9 March 2021

Publisher's Note: MDPI stays neutral with regard to jurisdictional claims in published maps and institutional affiliations.



Copyright: © 2021 by the authors. Licensee MDPI, Basel, Switzerland. This article is an open access article distributed under the terms and conditions of the Creative Commons Attribution (CC BY) license (<https://creativecommons.org/licenses/by/4.0/>).

1. Introduction

The electrical transport properties of the copper-oxide high- T_c superconductors (HTSCs) are strongly anisotropic because of their layered crystalline structure. Notably the Hall effect in these materials is one of the still unresolved fundamental puzzles. In the prototypical compound $\text{YBa}_2\text{Cu}_3\text{O}_{7-\delta}$ (YBCO) the Hall coefficient in the normal state changes in an unconventional manner by rotating the magnetic field. With the current injected along the CuO_2 layers and the magnetic field oriented perpendicular to the layers, a positive (hole-like) and strongly temperature dependent Hall effect is observed [1], but it is negative (electron-like) and temperature-independent over a wide range [2] when the magnetic field is oriented parallel to the layers and the Hall voltage is measured perpendicular to them. In both geometries, the magnetic field is oriented perpendicular to the current to maximize the Lorentz force on the charge carriers and the Hall field is probed orthogonally to both the current and magnetic field.

The Montgomery method [3] is commonly used to determine anisotropic electrical transport properties. However, with tiny single crystals, imperfections of the sample shape and the sizeable area of the contacts, as compared to the distance between them, introduce considerable uncertainty. Also, the density of the injected current varies strongly throughout the sample volume, which might be adverse for some investigations. Therefore, it would be of paramount importance to test and compare the anisotropic transport properties in an entirely different geometry.

The discovery of a huge Seebeck effect in $\text{YBa}_2\text{Cu}_3\text{O}_{7-\delta}$ films [4] has led to further investigations of the experimental opportunities of thin films grown on vicinal-cut substrates. The polished surface of a SrTiO_3 (STO) substrate, cut at a tilt angle α off the (001) plane,

shows a periodic nanoscale step structure. A subsequently deposited YBCO film replicates the surface steps and grows epitaxially in a self-organized roof-tile manner. For tilt angles $\alpha \leq 20^\circ$, a regular vicinal growth of the YBCO film and an approximately linear increase of the thermoelectric signal with α has been reported [5].

The morphology and defect microstructure of such vicinal YBCO films have been investigated in detail and the deviations from the idealized picture discussed [6–8]. High-resolution electron microscopy has revealed a bending of the YBCO lattice near the STO interface and the relaxation of these defects with increasing distance to the substrate. Correspondingly, the widths of x-ray diffraction rocking curves increase substantially in films with a thickness smaller than 200 nm [9].

Vicinal YBCO films show strong vortex pinning forces and an anisotropic critical current density [10,11] due to their parallel oriented planar defects. They are also useful for the deconvolution of angle-dependent critical current effects [12]. The reduced symmetry of vicinal films allows the observation of vortex channeling effects [13] when the magnetic field is parallel to the CuO_2 planes, which is not possible in c -axis oriented thin films. Another advantage of thin vicinal films is the access to out-of-plane transport properties in situations where the limited penetration depth of optical [14] or light ion irradiation [15] precludes the use of single crystals.

The anisotropic resistivities of several HTSCs thin films, grown on vicinal substrates, have been studied. Among them are optimally doped [6] and oxygen deficient YBCO [16], $\text{Bi}_2\text{Sr}_2\text{CaCu}_2\text{O}_8$ [17], $\text{Hg}_{1-x}\text{Re}_x\text{Ba}_2\text{CaCu}_2\text{O}_{6+\delta}$ [18], and, recently, the iron-based superconductors $\text{Fe}_{1+\delta}\text{Se}_{0.5}\text{Te}_{0.5}$ [19] and $\text{NdFeAs}(\text{O},\text{F})$ [20].

In this paper, we explore the anisotropic transport properties of a vicinal YBCO film and demonstrate that not only anisotropic resistivities but also the in-plane and out-of-plane Hall effect can be measured. Our results are supported by their good accordance with previous findings on single crystals.

2. Materials and Methods

2.1. Sample Preparation

Vicinal YBCO films are fabricated by pulsed-laser deposition (PLD) on off-axis cut SrTiO_3 substrates (TBL Kelpin, Neuhausen, Germany). One side face of the substrate is cut along the [100] direction but the surface normal is inclined at an angle $\alpha = 10^\circ$ towards the [010] direction. The polished substrates have a rms surface roughness of less than 0.2 nm. A (200 ± 20) nm thick YBCO film is grown by PLD with a KrF-excimer laser (LPX 305i, Coherent Inc., Santa Clara, CA, USA, Lambda Physik, Germany, $\lambda = 248$ nm, fluence 3.25 J/cm^2 , pulse duration 20 ns, repetition rate 10 Hz) from a stoichiometric YBCO target.

A high-resolution transmission electron microscopy (HRTEM) investigation of the interface microstructure of a similar vicinal YBCO thin film is shown in Figure 1 for two different cuts [9]. The interface between the SrTiO_3 substrate and the YBCO film is marked by white broken lines. In the cut perpendicular to the vicinal steps, a terraced surface of the substrate is evident in Figure 1a. The YBCO lattice is inclined by $\sim 10^\circ$ against the interface and exhibits a moderate density of stacking faults that relax with increasing distance to the interface. On the contrary, in a cut along the substrate terraces, the YBCO lattice is oriented parallel to the interface, as can be seen in Figure 1b.

The growth morphology of vicinal YBCO films is confirmed by comparing the X-ray diffraction (XRD) spectra (D8 GADDS Bruker Corp., Billerica, MA, USA) of a reference film on (100) SrTiO_3 substrate with that of a vicinal-grown YBCO film. The YBCO (001) diffraction peaks of both samples coincide when the vicinal substrate is tilted by 10° in the XRD chamber so that both samples are oriented identically with regard to the CuO_2 planes of YBCO [14]. Optical microscopy shows an even surface of our vicinal YBCO film, comparable to the surface

structure of c -axis oriented films. However, HRTEM investigations of our similarly fabricated vicinal films reveal terrace steps of 18 ± 6 nm height due to the bunching of several unit cells to a larger step [9].

After deposition, the film is patterned by standard photolithography and wet chemical etching into a cross-shaped geometry (see the inset in Figure 3) with two perpendicular bridges with length $l = 2.3$ mm and width $w = 0.1$ mm. Note that one bridge (A—B) is oriented parallel, the other (C—D) perpendicular to the terraces of the vicinal substrate. Finally, eight Au/Pd contact pads are evaporated for the electrical contacts and connected with Au wires.

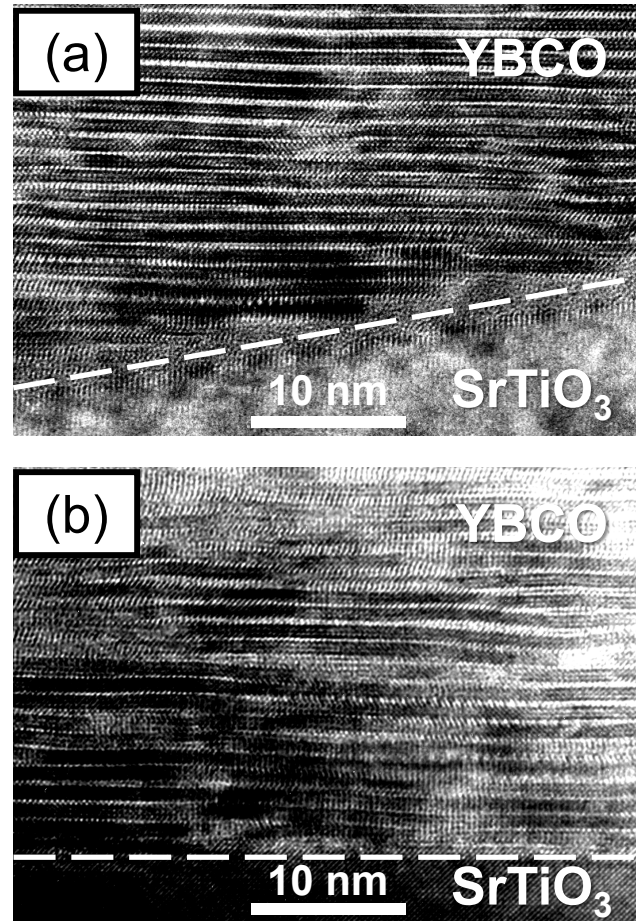


Figure 1. High-resolution transmission electron microscopy images of vicinal YBCO thin films near the substrate interface. (a) In a cut perpendicular to the vicinal steps, the crystal lattice of YBCO is inclined by $\sim 10^\circ$ relative to the substrate surface (indicated by a dashed line). (b) In a cut along the vicinal steps the YBCO lattice is oriented parallel to the substrate surface. Adapted from [9].

2.2. Transport Measurements

The electrical measurements are performed in a closed-cycle cryocooler mounted in a continuously rotatable electromagnet supplying a magnetic field of 1 T. A precise adjustment of the applied magnetic field orthogonal and parallel to the CuO_2 layers of the vicinal-grown YBCO film is achieved by monitoring the resistance at the low-temperature side of the superconducting transition as a function of the magnet rotation angle. During an extremely slow bidirectional temperature sweep (≤ 0.02 K/min) the data are collected at both polarities of the magnetic field by computer-controlled data acquisition using constant-amplitude ac current and a lock-in amplifier. The temperature was measured by a calibrated

platinum resistor in zero magnetic field and controlled by a Cernox resistor with negligible magnetoresistance [21].

2.3. Calculation of the Anisotropic Transport Properties

To evaluate the anisotropic transport parameters in vicinal films, two coordinate systems are introduced, as sketched in Figure 2. The orthogonal axes of the laboratory (substrate) system are labeled $\{x, y, z\}$ and are parallel to the substrate edges, while the crystallographic axes of YBCO are labeled $\{a, b, c\}$. Only the resistivity tensor ρ_{xyz} in the substrate system is experimentally accessible and is connected to the resistivity tensor ρ_{abc} of the YBCO film via the rotational transformation matrix R of the coordinates

$$\rho_{xyz} = R \rho_{abc} R^{-1}, \quad (1)$$

where in our vicinal film, $a \parallel x$ and $b \perp c$ are rotated by the vicinal angle α around the x -axis, hence

$$R_x(\alpha) = \begin{pmatrix} 1 & 0 & 0 \\ 0 & \cos \alpha & -\sin \alpha \\ 0 & \sin \alpha & \cos \alpha \end{pmatrix}, \quad R_x^{-1}(\alpha) = \begin{pmatrix} 1 & 0 & 0 \\ 0 & \cos \alpha & \sin \alpha \\ 0 & -\sin \alpha & \cos \alpha \end{pmatrix}. \quad (2)$$

The resistivity tensors in the substrate and the sample systems are, respectively,

$$\rho_{xyz} = \begin{pmatrix} \rho_{xx} & \rho_{xy} & \rho_{xz} \\ \rho_{yx} & \rho_{yy} & \rho_{yz} \\ \rho_{zx} & \rho_{zy} & \rho_{zz} \end{pmatrix}, \quad \rho_{abc} = \begin{pmatrix} \rho_{aa} & -\rho_{ba} & -\rho_{ca} \\ \rho_{ba} & \rho_{aa} & -\rho_{cb} \\ \rho_{ca} & \rho_{cb} & \rho_{cc} \end{pmatrix}, \quad (3)$$

where the latter has been simplified by considering the tensor symmetry $\rho_{ik} = -\rho_{ki}$, $i \neq k \in \{a, b, c\}$ according to the Onsager reciprocity relationship [22]. In materials with tetragonal crystalline symmetry $\rho_{bb} \simeq \rho_{aa}$. Although YBCO has orthogonal symmetry, the twinning in our YBCO films leads to a quasi-tetragonal behavior at the length scales of transport measurements. The relevant components of ρ_{xyz} are then

$$\rho_{xx} = \rho_{aa}, \quad (4)$$

$$\rho_{yy} = \rho_{aa} \cos^2 \alpha + \rho_{cc} \sin^2 \alpha, \quad (5)$$

$$\rho_{yx} = -\rho_{xy} = \rho_{ba} \cos \alpha - \rho_{ca} \sin \alpha, \quad (6)$$

$$\rho_{zx} = -\rho_{xz} = \rho_{ba} \sin \alpha + \rho_{ca} \cos \alpha, \quad (7)$$

$$\rho_{yz} = -\rho_{zy} = \rho_{aa} \sin \alpha \cos \alpha - \rho_{cc} \sin \alpha \cos \alpha - \rho_{cb}. \quad (8)$$

Several conditions are essential for reliable measurements of vicinal films. The required high level of crystallinity and epitaxial growth of the films sets an upper limit for the vicinal angle $\alpha \leq 20^\circ$ in YBCO [5]. Conversely, α should not be too small to allow for an adequate sensitivity of the measurements. Then, the various elements of the resistivity tensor can be determined by applying a current density j_k , in selected directions and measuring the resulting electric field component E_i according to Ohm's law

$$E_i = \rho_{ik} j_k, \quad i, k \in \{x, y, z\}. \quad (9)$$

2.3.1. Evaluation of Diagonal Resistivity Tensor Elements

When a current density j_x is injected via the contacts A and B, the resulting electric field probed between contacts A' and B' follows from Equations (4) and (9)

$$E_x = \rho_{xx}j_x + \underbrace{\rho_{xy}j_y}_{j_y=0} + \underbrace{\rho_{xz}j_z}_{j_z=0} = \rho_{aa}j_x \quad (10)$$

and thus $\rho_{aa} = \rho_{xx}$.

Alternatively, a current density j_y applied via contacts C and D results in an electric field E_y between contacts C' and D'

$$E_y = \underbrace{\rho_{yx}j_x}_{j_x=0} + \rho_{yy}j_y + \underbrace{\rho_{yz}j_z}_{j_z=0} = (\rho_{aa} \cos^2 \alpha + \rho_{cc} \sin^2 \alpha)j_y \quad (11)$$

according to Equations (5) and (9). By combining Equations (10) and (11) the out-of-plane resistivity of the vicinal film can be calculated from two measurements

$$\rho_{cc} = (\rho_{yy} - \rho_{xx} \cos^2 \alpha) / \sin^2 \alpha. \quad (12)$$

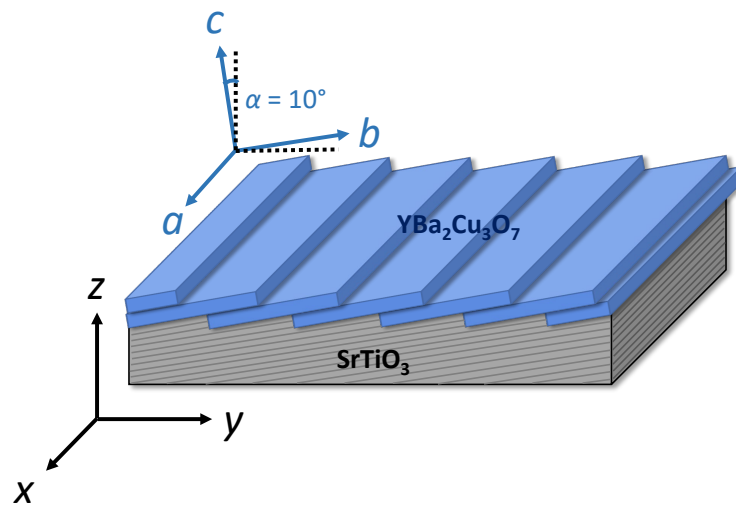


Figure 2. Substrate and YBCO coordinate systems in thin films grown on vicinal-cut substrates. The two coordinate systems are rotated by an angle α around the x axis.

2.3.2. Evaluation of off-Diagonal (Hall) Tensor Elements

Applying a magnetic field \mathbf{B} gives rise to nonzero off-diagonal elements of the resistivity tensors Equation (3) that depend on the magnitude and orientation of \mathbf{B} . Here, only the terms to the first order in \mathbf{B} are considered that are evoked by the Lorentz force acting on the charge carriers. For simplicity of the evaluation, Hall effect experiments are commonly designed such that $\mathbf{E} \perp \mathbf{j} \perp \mathbf{B}$. With a substrate surface oriented parallel to the xy plane it would require $\mathbf{B} = (0, 0, B_z)$.

However, two arguments suggest aligning \mathbf{B} parallel or perpendicular to the crystallographic ab plane instead. First, the vortex lock-in transition [23,24] allows one to accurately adjust \mathbf{B} parallel to the CuO_2 planes of YBCO, irrespective of any misorientation of the substrate in the cryostat or uncertainties of the vicinal growth angle α . Second, evaluation of the Hall coefficients $R_{ik}^H = \rho_{ik}/B_l, i \neq k \neq l \in \{a, b, c\}$ in the crystallographic system becomes simpler since the tensor components $\rho_{ik} = 0$ in a magnetic field B_l such that $i = l$. This reflects the absence of Lorentz force for the current component that is parallel to the magnetic field.

Then, the in-plane Hall coefficient $R_{ba}^H = -R_{ab}^H$ and the out-of-plane Hall coefficient $R_{ca}^H = -R_{ac}^H$ can be determined each with two independent measurements:

$$\rho_{yx} = \frac{E_y}{j_x} = \underbrace{\rho_{ba} \cos \alpha}_{\rho_{ba}=0} - \rho_{ca} \sin \alpha = -R_{ca}^H B_b \sin \alpha, \quad B_a = B_c = 0, \quad (13)$$

$$\rho_{yx} = \frac{E_y}{j_x} = \rho_{ba} \cos \alpha - \underbrace{\rho_{ca} \sin \alpha}_{\rho_{ca}=0} = R_{ba}^H B_c \cos \alpha, \quad B_a = B_b = 0, \quad (14)$$

$$\rho_{xy} = \frac{E_x}{j_y} = \rho_{ca} \sin \alpha - \underbrace{\rho_{ba} \cos \alpha}_{\rho_{ba}=0} = R_{ca}^H B_b \sin \alpha, \quad B_a = B_c = 0, \quad (15)$$

$$\rho_{xy} = \frac{E_x}{j_y} = \underbrace{\rho_{ca} \sin \alpha}_{\rho_{ca}=0} - \rho_{ba} \cos \alpha = -R_{ba}^H B_c \cos \alpha, \quad B_a = B_b = 0. \quad (16)$$

3. Results and Discussion

Figure 3 presents the temperature dependencies of the in-plane resistivity ρ_{aa} and the resistivity perpendicular to the CuO_2 layers ρ_{cc} of the optimally doped YBCO thin film grown on a $\alpha = 10^\circ$ vicinal SrTiO_3 substrate. While $\rho_{aa} = \rho_{xx}$ can be directly determined from one measurement, ρ_{cc} is calculated according to Equation (12) from two measurements employing current along the x and y axes, respectively. The normal-state resistivity ρ_{aa} has a linear temperature dependence, which extrapolates to an offset $\rho_{aa}(0\text{ K}) \sim -1 \mu\Omega \text{ cm}$. At $T \lesssim 110\text{ K}$ ρ_{aa} falls below the linear trend because of the paraconductivity stemming from superconducting order-parameter fluctuations [25].

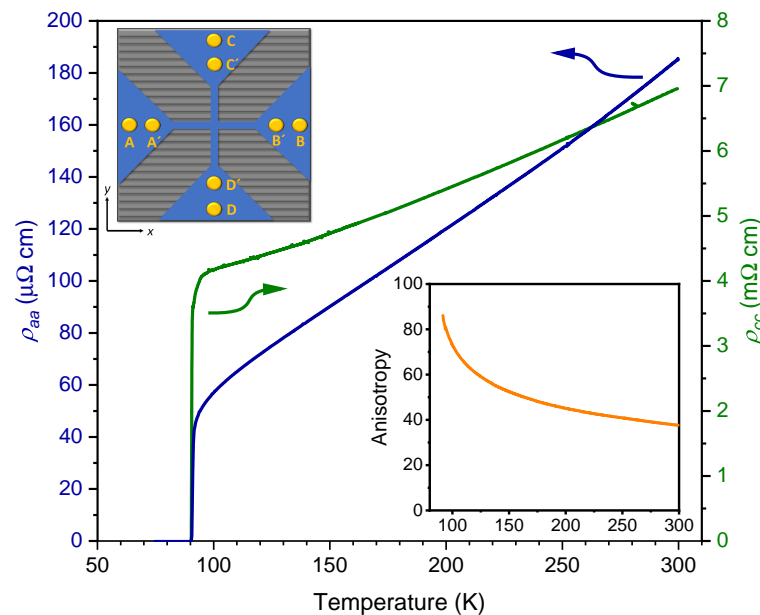


Figure 3. Temperature dependence of the in-plane resistivity ρ_{aa} (blue line) and out-of-plane resistivity ρ_{cc} (green line) of an optimally doped YBCO thin film grown on a $\alpha = 10^\circ$ vicinal substrate. Bottom right inset: Resistivity anisotropy $\gamma = \rho_{cc}/\rho_{aa}$ as a function of temperature. Top left inset: Schematic view of the cross-shaped patterned YBCO film (blue). Grey lines indicate the terraced structure of the SrTiO₃ substrate. Current can be applied in either x direction via contacts (yellow) A—B, or along the y direction via contacts C—D. The neighboring inner contacts (A' and B' or C' and D') are used for resistivity measurements, while for probing the Hall voltage the contacts on the bridge orthogonal to the current flow are used. In parts adapted from [16].

The out-of-plane normal-state resistivity ρ_{cc} has a metallic temperature dependence, too, in contrast to oxygen-depleted YBCO [26] and HTSCs with stronger anisotropy like Bi₂Sr₂CaCu₂O₈ [27]. The bottom right inset in Figure 3 displays the increase of the resistivity anisotropy $\gamma = \rho_{cc}/\rho_{aa}$ from $\gamma(300\text{ K}) = 38$ to $\gamma(100\text{ K}) = 73$ when reducing the temperature. Both ρ_{aa} and ρ_{cc} vanish at $T_{c0} = 90.3\text{ K}$.

It is instructive to compare the present results obtained in the vicinal film with those in YBCO single crystals and c -axis oriented thin films. The in-plane resistivity at room temperature $\rho_{aa}(300\text{ K}) = 185\ \mu\Omega\text{ cm}$ is only marginally larger than previously reported for twinned [28] and untwinned [29] single crystals, if compared to the average value $(\rho_{aa} + \rho_{bb})/2 \simeq 165\ \mu\Omega\text{ cm}$ of the latter. An intercept of the extrapolated normal-state resistivity $\rho_{aa}(0\text{ K})$ close to zero or even at slightly negative values of $\rho_{aa}(0\text{ K})$ is commonly considered a sign of a low density of structural defects [30]. Conversely, introducing oxygen disorder enhances the offset, while leaving the slope of $\rho_{aa}(T)$ almost unchanged [31,32].

The out-of-plane resistivity ρ_{cc} of YBCO determined in our vicinal film corresponds intriguingly well with data obtained in twinned single crystals [33], both regarding the absolute value and the metallic temperature dependence. It has been proposed that an extended Mott-Ioffe-Regel limit $\rho_{cc}^M \sim 10\text{ m}\Omega\text{ cm}$ bifurcates between HTSCs with metallic behavior when $\rho_{cc}(T) < \rho_{cc}^M$ and semiconducting behavior if $\rho_{cc}(T) > \rho_{cc}^M$ [26]. The latter applies to most of the HTSCs. From Figure 3 it is evident that ρ_{cc} falls only marginally below this limit and, indeed, in slightly oxygen-depleted YBCO ($\delta = 0.13$) with $\rho_{cc}(300\text{ K}) \sim \rho_{cc}^M$ a semiconducting behavior is observed. Early experiments in YBCO single crystals also reported somewhat higher $\rho_{cc}(T)$ and a semiconducting behavior below 200 K [1,34]. Hence, the results

for both out-of-plane and in-plane resistivities in our vicinal films are well comparable to those in optimally doped YBCO single crystals.

The in-plane Hall coefficient R_{ba}^H , measured with the magnetic field oriented parallel to the crystallographic c axis and evaluated according to Equation (16), is presented in Figure 4. Like in single crystals [1,2,33] and c -axis oriented thin films [25], R_{ba}^H of our vicinal YBCO film is positive (hole-like) and increases towards lower temperatures, followed by a sharp drop slightly above T_c as a consequence of the onset of superconducting order parameter fluctuations [25]. A second set of data can be obtained by evaluating Equation (14) yielding consistent results, but with a worse signal to noise ratio (grey triangles).

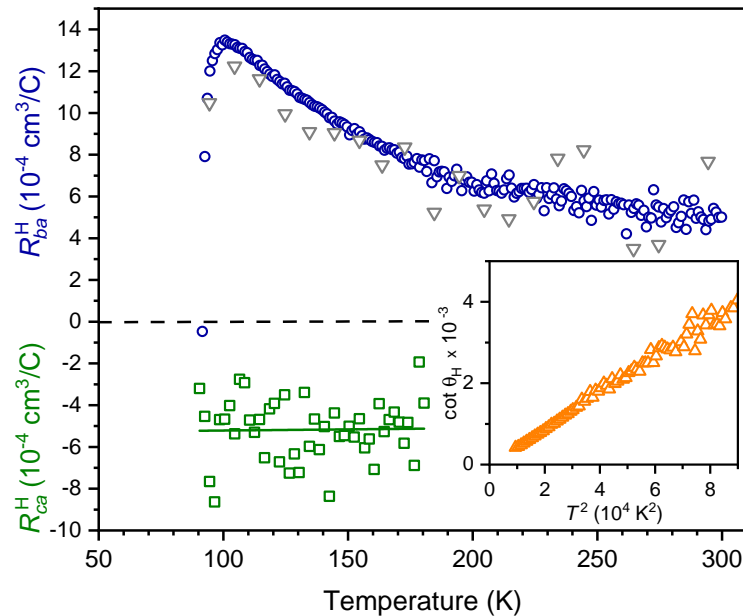


Figure 4. Temperature dependence of the anisotropic Hall effect in a vicinal YBCO film. The in-plane Hall coefficient R_{ba}^H evaluated from Equation (16) and averaged to 1 K intervals is shown by blue circles. Grey triangles represent the alternative evaluation by Equation (14), averaged to 10 K intervals. The out-of-plane Hall coefficient R_{ca}^H (green squares) is determined by Equation (15) and averaged into 2 K intervals. The full line is a linear fit to the data. Inset: Cotangent of the in-plane Hall angle θ_H vs. square of the temperature.

The inset of Figure 4 confirms that the in-plane Hall angle $\tan \theta_H = R_{ba}^H B_c / \rho_{aa}$ follows Anderson's law [35] $\cot \theta_H = AT^2 + C$, where C is proportional to the density of carrier scattering defects and A is a measure of the carrier density. A linear relation between $\cot \theta_H$ and T^2 can be observed in the temperature range from ~ 100 K to 300 K. The intercept $C \sim 0$, indicating a minor number of carrier scattering defects—a finding that is also supported by the small intercept of ρ_{aa} discussed above.

A different measurement setup with the magnetic field $\mathbf{B} = (0, B_b, 0)$ oriented parallel to CuO_2 planes allows for the evaluation of the out-of-plane Hall coefficient R_{ca}^H according to Equation (15). In sharp contrast to the positive in-plane Hall effect, the out-of-plane Hall coefficient $R_{ca}^H \sim -5 \times 10^{-4}$ cm³/C is negative and almost temperature independent, as can be seen in Figure 4. The straight line is a linear fit to the data, which does not reveal any temperature dependence, although a slight reduction of R_{ca}^H at lower temperatures cannot be ruled out due to the scatter of data points. Above 180 K the noise was too large to provide reliable data. The alternative evaluation of R_{ca}^H by Equation (13) confirms its negative sign but was not accurate enough to allow for a quantitative statement. Using films with a larger

vicinal angle α would increase the signal-to-noise ratio on the cost of a less regular growth of the YBCO layers, presumably counteracting the advantages of larger signals.

Although the apparent discrepancy of the anisotropic Hall effect in YBCO to conventional transport theory has spurred intense discussions, only few measurements in YBCO single crystals are available. In this respect our investigations on a vicinal film provide a complementary and entirely different measurement method. Our findings for the out-of-plane Hall effect are in good accordance with earlier results on YBCO single crystals, which indicated a slightly temperature dependent $R_{ca}^H \sim -7.5 \times 10^{-4}$ to $-9 \times 10^{-4} \text{ cm}^3/\text{C}$ [1], a temperature independent $R_{ca}^H \sim -6.2 \times 10^{-4} \text{ cm}^3/\text{C}$ between 100 K and 400 K [2], and $R_{ca}^H \sim -4.2 \times 10^{-4} \text{ cm}^3/\text{C}$ at 100 K [36].

4. Conclusions

Thin films of YBCO, grown on vicinal-cut SrTiO₃ substrates, show anisotropic transport properties when the current is injected either parallel or perpendicular to the growth terraces. From these data, the resistivities parallel and orthogonal to the CuO₂ layers can be calculated. The results are in excellent agreement with data in single crystals.

By applying a magnetic field either perpendicular or parallel to the CuO₂ layers the in-plane and the out-of-plane Hall effect can be obtained, respectively. The results are in excellent agreement with single crystal data and confirm the puzzling disparity of in-plane and out-of-plane Hall coefficients regarding their sign and temperature dependence.

We conclude that magneto-transport measurements in vicinal films of layered materials yield equivalent results to measurements in single crystals. The former offer several advantages, like a better controllable sample geometry and a well-defined homogeneous current density. In this respect, vicinal thin films of various superconductors, from copper-oxide to iron-based compounds, might be helpful to study their anisotropic transport properties. Moreover, vicinal thin films are useful for investigations, where a limited penetration depth of photons or ions with moderate energy precludes the use of single crystals.

Author Contributions: W.L. and J.D.P. conceived and supervised the experiments, R.R. and J.D.P. grew and characterized the film, G.H. performed the transport measurements and the analysis, all authors discussed the results, W.L. wrote the paper with substantial contributions from G.H. All authors have read and agreed to the published version of the manuscript.

Funding: This research was funded by the Austrian Science Fund (FWF) under grant I4865-N and the COST Actions CA16218 (NANOCOBYBRI) and CA19108 (Hi-SCALE) of the European Cooperation in Science and Technology.

Data Availability Statement: The data presented in this study are available on reasonable request from the corresponding author.

Conflicts of Interest: The authors declare no conflict of interest.

References

1. Tozer, S.W.; Penney, T.; Kaiser, D.; Holtzberg, F. Measurement of Anisotropic Resistivity and Hall Constant for Single-Crystal YBa₂Cu₃O_{7-x}. *Phys. Rev. Lett.* **1987**, *59*, 1768–1771. [[CrossRef](#)]
2. Harris, J.M.; Yan, Y.F.; Ong, N.P. Experimental Test of the T^2 Law for the Hall Angle from T_c to 500 K in Oxygen-Reduced YBa₂Cu₃O_{6+x} Crystals. *Phys. Rev. B* **1992**, *46*, 14293–14296. [[CrossRef](#)] [[PubMed](#)]
3. Montgomery, H.C. Method for Measuring Electrical Resistivity of Anisotropic Materials. *J. Appl. Phys.* **1971**, *42*, 2971–2975. [[CrossRef](#)]
4. Lengfellner, H.; Kremb, G.; Schnellbögl, A.; Betz, J.; Renk, K.F.; Prettl, W. Giant Voltages Upon Surface Heating in Normal YBa₂Cu₃O_{7- δ} Films Suggesting an Atomic Layer Thermopile. *Appl. Phys. Lett.* **1992**, *60*, 501–503. [[CrossRef](#)]
5. Lengfellner, H.; Zeuner, S.; Prettl, W.; Renk, K.F. Thermoelectric Effect in Normal-State YBa₂Cu₃O_{7- δ} Films. *Europhys. Lett.* **1994**, *25*, 375–378. [[CrossRef](#)]
6. Haage, T.; Zegenhagen, J.; Li, J.Q.; Habermeier, H.U.; Cardona, M.; Warthmann, J.R.; Forkl, A.; Kronmüller, H. Transport properties and flux pinning by self-organization in YBa₂Cu₃O_{7- δ} films on vicinal SrTiO₃ (001). *Phys. Rev. B* **1997**, *56*, 8404–8418. [[CrossRef](#)]

7. Méchin, L.; Berghuis, P.; Evetts, J.E. Properties of $\text{YBa}_2\text{Cu}_3\text{O}_{7-\delta}$ thin films grown on vicinal SrTiO_3 (001) substrates. *Phys. C* **1998**, *302*, 102–112. [[CrossRef](#)]
8. Maurice, J.L.; Briatico, J.; Crété, D.G.; Contour, J.P.; Durand, O. Effects of surface miscuts on the epitaxy of $\text{YBa}_2\text{Cu}_3\text{O}_{7-\delta}$ and $\text{NdBa}_2\text{Cu}_3\text{O}_{7-\gamma}$ on SrTiO_3 (001). *Phys. Rev. B* **2003**, *68*, 115429. [[CrossRef](#)]
9. Pedarnig, J.D.; Rössler, R.; Delamare, M.P.; Lang, W.; Bäuerle, D.; Köhler, A.; Zandbergen, H.W. Electrical properties, texture, and microstructure of vicinal $\text{YBa}_2\text{Cu}_3\text{O}_{7-\delta}$ thin films. *Appl. Phys. Lett.* **2002**, *81*, 2587–2589. [[CrossRef](#)]
10. Jooss, C.; Warthmann, R.; Kronmüller, H.; Haage, T.; Habermeier, H.U.; Zegenhagen, J. Vortex pinning due to strong quasiparticle scattering at antiphase boundaries in $\text{YBa}_2\text{Cu}_3\text{O}_{7-\delta}$. *Phys. Rev. Lett.* **1999**, *82*, 632–635. [[CrossRef](#)]
11. Emergo, R.L.S.; Wu, J.Z.; Aytug, T.; Christen, D.K. Thickness dependence of superconducting critical current density in vicinal $\text{YBa}_2\text{Cu}_3\text{O}_{7-\delta}$ thick films. *Appl. Phys. Lett.* **2004**, *85*, 618–620. [[CrossRef](#)]
12. Durrell, J.H.; Burnell, G.; Tsaneva, V.N.; Barber, Z.H.; Blamire, M.G.; Evetts, J.E. Critical currents in vicinal $\text{YBa}_2\text{Cu}_3\text{O}_{7-\delta}$ films. *Phys. Rev. B* **2004**, *70*, 214508. [[CrossRef](#)]
13. Berghuis, P.; Di Bartolomeo, E.; Wagner, G.A.; Evetts, J.E. Intrinsic channeling of vortices along the *ab* plane in vicinal $\text{YBa}_2\text{Cu}_3\text{O}_{7-\delta}$ films. *Phys. Rev. Lett.* **1997**, *79*, 2332–2335. [[CrossRef](#)]
14. Markowitsch, W.; Stockinger, C.; Lang, W.; Bierleutgeb, K.; Pedarnig, J.D.; Bäuerle, D. Photoinduced enhancement of the c-axis conductivity in oxygen-deficient $\text{YBa}_2\text{Cu}_3\text{O}_{7-\delta}$ thin films. *Appl. Phys. Lett.* **1997**, *71*, 1246–1248. [[CrossRef](#)]
15. Lang, W.; Richter, H.; Marksteiner, M.; Siraj, K.; Bodea, M.A.; Pedarnig, J.D.; Grigoropoulos, C.; Bäuerle, D.; Hasenfuss, C.; Palmethofer, L.; et al. Masked ion beam irradiation of high-temperature superconductors: patterning of nano-size regions with high point-defect density. *Int. J. Nanotechnol.* **2009**, *6*, 704–714. [[CrossRef](#)]
16. Heine, G.; Lang, W.; Rössler, R.; Pedarnig, J.D.; Bäuerle, D. Sign change of the out-of-plane magnetoresistance in oxygen-deficient YBCO. *J. Low Temp. Phys.* **1999**, *117*, 1265–1269. [[CrossRef](#)]
17. Li, S.; Ritzer, A.; Arenholz, E.; Bäuerle, D.; Huber, W.; Lengfellner, H.; Prettl, W. Step-like growth of $\text{Bi}_2\text{Sr}_2\text{CaCu}_2\text{O}_8$ films on off-axis oriented (001) SrTiO_3 . *Appl. Phys. A* **1996**, *63*, 427–429. [[CrossRef](#)]
18. Yun, S.H.; Pedarnig, J.D.; Rössler, R.; Bäuerle, D.; Obradors, X. In-plane and out-of-plane resistivities of vicinal Hg-1212 thin films. *Appl. Phys. Lett.* **2000**, *77*, 1369–1371. [[CrossRef](#)]
19. Bryja, H.; Hühne, R.; Iida, K.; Molatta, S.; Sala, A.; Putti, M.; Schultz, L.; Nielsch, K.; Hänisch, J. Deposition and properties of Fe(Se,Te) thin films on vicinal CaF_2 substrates. *Supercond. Sci. Technol.* **2017**, *30*, 115008. [[CrossRef](#)]
20. Iida, K.; Matsumoto, T.; Kondo, K.; Hatano, T.; Ikuta, H. Anisotropy of the transport properties of $\text{NdFeAs}(\text{O},\text{F})$ thin films grown on vicinal substrates. *Supercond. Sci. Technol.* **2020**, *33*, 044016. [[CrossRef](#)]
21. Heine, G.; Lang, W. Magnetoresistance of the new ceramic ‘Cernox’ thermometer from 4.2 K to 300 K in magnetic fields up to 13 T. *Cryogenics* **1998**, *38*, 377–379. [[CrossRef](#)]
22. Onsager, L. Reciprocal relations in irreversible processes. II. *Phys. Rev.* **1931**, *38*, 2265–2279. [[CrossRef](#)]
23. Tachiki, M.; Takahashi, S. Strong Vortex Pinning Intrinsic in High- T_c Oxide Superconductors. *Solid State Commun.* **1989**, *70*, 291–295. [[CrossRef](#)]
24. Feinberg, D.; Villard, C. Intrinsic Pinning and Lock-in Transition of Flux Lines in Layered Type-II Superconductors. *Phys. Rev. Lett.* **1990**, *65*, 919–922. [[CrossRef](#)] [[PubMed](#)]
25. Lang, W.; Heine, G.; Schwab, P.; Wang, X.Z.; Bäuerle, D. Paraconductivity and Excess Hall Effect in Epitaxial $\text{YBa}_2\text{Cu}_3\text{O}_7$ Films Induced by Superconducting Fluctuations. *Phys. Rev. B* **1994**, *49*, 4209–4217. [[CrossRef](#)]
26. Ito, T.; Takagi, H.; Ishibashi, S.; Ido, T.; Uchida, S. Normal-State Conductivity Between CuO_2 Planes in Copper Oxide Superconductors. *Nature* **1991**, *350*, 596–598. [[CrossRef](#)]
27. Heine, G.; Lang, W.; Wang, X.L.; Dou, S.X. Positive in-plane and negative out-of-plane magnetoresistance in the overdoped high-temperature superconductor $\text{Bi}_2\text{Sr}_2\text{CaCu}_2\text{O}_{8+x}$. *Phys. Rev. B* **1999**, *59*, 11179–11182. [[CrossRef](#)]
28. Winzer, K.; Kumm, G. Fluctuation-Enhanced Conductivity and Magnetoconductivity of High-Quality $\text{YBa}_2\text{Cu}_3\text{O}_{7-\delta}$ Crystals. *Z. Phys. B* **1991**, *82*, 317–321. [[CrossRef](#)]
29. Rice, J.; Giapintzakis, J.; Ginsberg, D.; Mochel, J. Hall Effect Above T_c in Untwinned Single-Crystal $\text{YBa}_2\text{Cu}_3\text{O}_{7-x}$: Normal-State Behavior and Superconducting Fluctuations. *Phys. Rev. B* **1991**, *44*, 10158–10166. [[CrossRef](#)]
30. Chien, T.R.; Wang, Z.Z.; Ong, N.P. Effect of Zn Impurities on the Normal-State Hall Angle in Single-Crystal $\text{YBa}_2\text{Cu}_{3-x}\text{Zn}_x\text{O}_{7-\delta}$. *Phys. Rev. Lett.* **1991**, *67*, 2088–2091. [[CrossRef](#)] [[PubMed](#)]
31. Wang, X.Z.; Hellebrand, B.; Bäuerle, D.; Strecker, M.; Wortmann, G.; Lang, W. Oxygen ordering and superconductivity in $\text{GdBaSrCu}_3\text{O}_{7-x}$. *Phys. C* **1995**, *242*, 55–62. [[CrossRef](#)]
32. Lang, W.; Pedarnig, J.D. Ion Irradiation of High-Temperature Superconductors and Its Application for Nanopatterning. In *Nanoscience and Engineering in Superconductivity*; Moshchalkov, V.V., Würdenweber, R., Lang, W., Eds.; Springer: Berlin/Heidelberg, Germany, 2010; pp. 81–104. [[CrossRef](#)]
33. Holm, W.; Andersson, M.; Rapp, Ö.; Kulikov, M.A.; Makarenko, I.N. Anisotropic Fluctuation Magnetoconductivity in a $\text{YBa}_2\text{Cu}_3\text{O}_{7-\delta}$ Single Crystal Above T_c . *Phys. Rev. B* **1993**, *48*, 4227–4230. [[CrossRef](#)] [[PubMed](#)]

34. Penney, T.; von Mólnar, S.; Kaiser, D.; Holtzberg, F.; Kleinsasser, A.W. Strongly Anisotropic Electrical Properties of Single-Crystal $\text{YBa}_2\text{Cu}_3\text{O}_{7-x}$. *Phys. Rev. B* **1988**, *38*, 2918. [[CrossRef](#)]
35. Anderson, P.W. Hall effect in the two-dimensional Luttinger liquid. *Phys. Rev. Lett.* **1991**, *67*, 2092–2094. 67.2092. [[CrossRef](#)] [[PubMed](#)]
36. Eltsev, Y.; Rapp, Ö. Out-of-plane Hall effect in $\text{YBa}_2\text{Cu}_3\text{O}_{7-\delta}$: Vortex-glass behavior and scaling of *c*-axis and Hall resistivities. *Phys. Rev. B* **1998**, *57*, R3237–R3240. [[CrossRef](#)]